Resource-mediated competition between two plant species with different rates of water intake

Chunyi Gai and Theodore Kolokolnikov
Department of Mathematics and Statistics, Dalhousie University, Halifax, Canada

We propose an extension of the well-known Klausmeier model of vegetation to two plant species that consume water at different rates. Rather than competing directly, the plants compete through their intake of water, which is a shared resource between them. In semi-arid regions, the Klausmeier model produces vegetation spot patterns. We are interested in how the competition for water affects co-existence and stability of patches of different plant species. We consider two plant types: a "thirsty" species and a "frugal" species, that only differ by the amount of water they consume, while being identical in all other aspects. We find that there is a finite range of precipitation rate for which two species can co-exist. Outside of that range, (when the rate is either sufficiently low or high), the frugal species outcompetes the thirsty species. As the precipitation rate is decreased, there is sequence of stability thresholds such that thirsty plant patches are the first to die off, while the frugal spots remain resilient for longer. The pattern consisting of only frugal spots is the most resilient. The next-most-resilient pattern consists of all-thirsty patches, with the mixed pattern being less resilient than either of the homogeneous patterns. We also examine numerically what happens for very large precipitation rate. We find that for sufficiently high rate, the frugal plant takes over the entire range, outcompeting the thirsty plant.

1. INTRODUCTION

Competition for resources has long been regarded as one of the main mechanisms in structuring plant communities and natural selection [1–3]. In particular, in the semiarid regions where water resource is limited, the sparsity of water can lead to self-organised vegetation patterns such as vegetation patches and stripes [4–9]. These patterns can be thought of as a transition state from full vegetation to a desert state [5, 9–13].

In this paper, we look at competition for water between two plant species with different water absorption rates in the water-limited regime, where the vegetation is patches form. We are interested in how the competition for water affects co-existence and stability of patches of different plant species. We consider two plant species: a "thirsty" species and a "frugal" species, that only differ by the amount of water they consume, while being identical in all other aspects.

Our starting point is the following variant of the Klausmeier model, incoroporating two plant species and water-mediated competition between them:

$$\begin{aligned} \partial_t u_1 &= D_u \partial_{xx} u_1 - \mu u_1 + \gamma u_1^2 v, \\ \partial_t u_2 &= D_u \partial_{xx} u_2 - \mu u_2 + \gamma u_2^2 v, \\ \partial_t v &= D_v \partial_{xx} v + a - c_1 u_1^2 v - c_2 u_2^2 v. \end{aligned} \tag{1.1}$$

Here, u_1 and u_2 represent plant densities of the two types of plants and v denotes the concentration of the water in the soil. For simplicity and concreteness, we will consider their dynamics to be identical, except for the amount of water consumed per unit growth. We take these dynamics as originally suggested by Klausmeier [4]. In the absence of water, the plants wither with a rate μ. They grow at the same rate $\gamma u_i v$ in the presence of water. Plants "diffuse" through seed dispersal in proportion to the diffusion constant D_u. The water diffuses through the soil according to the diffusion constant D_v. The constants c_1, c_2 represent the amount of water intake needed to grow at a given rate γ. The term a represents water precipitation. The plant species u_1 is more thirsty than u_2 if $c_1 > c_2$.

By rescaling, we reduce (1.1) to the following non-dimensional form [1]

$$\begin{aligned} \partial_t u_1 &= \varepsilon^2 \partial_{xx} u_1 - u_1 + u_1^2 v, \\ \partial_t u_2 &= \varepsilon^2 \partial_{xx} u_2 - u_2 + u_2^2 v, \\ \tau \partial_t v &= D \partial_{xx} v + a - \frac{u_1^2 v}{\varepsilon} - \beta \frac{u_2^2 v}{\varepsilon}, \end{aligned} \tag{1.2}$$

which we will refer to as the "two-species vegetation model". Here, $\beta = c_2/c_1$ is the ratio of the water intake rates. In what follows, we will assume that $D \gg O(\varepsilon^2)$ and τ is sufficiently small that the term $\tau \partial_t v$ doesn't affect the

---

[1] Take $\mu, \gamma = 1$ by rescaling the time variable t and relabelling parameters. Next, let $\varepsilon := \sqrt{D_u}$ and rescale $u_1 = \hat{u}_1 \frac{1}{c_1 \varepsilon}$, $u_2 = \hat{u}_2 \frac{1}{c_1 \varepsilon}$, $v = \hat{v} c_1 \varepsilon$. Dropping the hats yields (1.2) with $\tau = \varepsilon c_1$, $D = D_v \varepsilon c_1$.

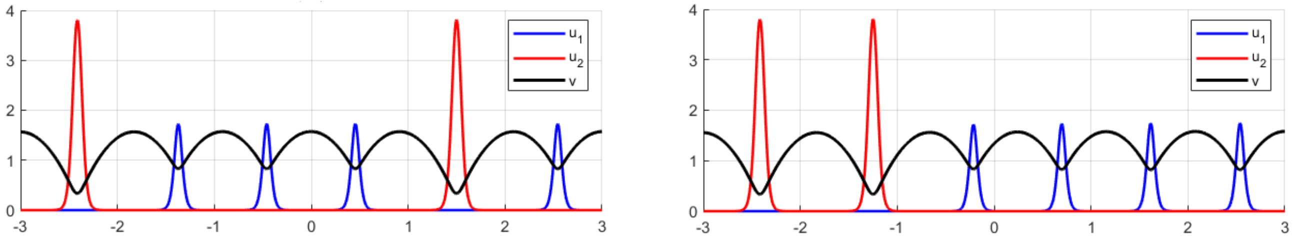

FIG. 1. Two steady states of (1.2), consisting of $k_1 = 4$ spikes of type u_1 (blue) and $k_2 = 2$ spikes of type u_2 (red). Parameters are $\varepsilon = 0.025, a = 8, L = 3, D = 1, \beta = 0.5$. The spike heights and profiles are the same for each type, regardless of the spike ordering.

dynamics and can be discarded to leading order. In terms of the original variables, these assumptions reflect the fact that the "diffusion" of plants through seed dispersal is on a much slower scale than the water diffusion through the soil. We will also assume Neumann boundary conditions on a domain $x \in (-L, L)$:

$$\partial_x u_1(\pm L) = \partial_x u_2(\pm L) = \partial_x v(\pm L) = 0. \tag{1.3}$$

The ratio β indicates how thirsty is plant species u_1 compared to u_2. When $\beta < 1$, the species u_2 consumes less water than u_1, and the opposite is true when $\beta > 1$. Without the generality, we may also assume that $0 < \beta \leq 1$, so that u_1 is more thirsty (per unit growth) than u_2 : u_1 is the "thirsty" species whereas u_2 is the "frugal" species in such a case.

When $\beta = 1$, the two species are indistinguishable from each-other, and the model (1.2) *behaves* like the "classical" Schnakenberg model [14, 15],

$$\partial_t u = \varepsilon^2 \partial_{xx} u - u + u^2 v, \qquad \tau \partial_t v = D\partial_{xx} v + a - \frac{u^2 v}{\varepsilon} \tag{1.4}$$

where $u = u_1 + u_2$ (this model is itself a special case of the Klausmeier model).

In this paper, we will be concerned with the following parameter regime

$$0 < \varepsilon \ll 1, \quad \tau = 0; \quad D, a = O(1). \tag{1.5}$$

The assumption $\tau = 0$ can be replaced with "$\tau \ll D$" without any change in the results.

It is well documented that Schnakenberg model (1.4) admits spot solutions having N concentrations in u [14, 15]. More generally, similar results for spike-stability analysis are obtained in singularly perturbed two-component reaction diffusion systems such as Schnakenberg model, Gierer-Meinhardt model [16, 17], and the Gray-Scott model [18–21]. However there are important differences both in the analysis and in the stability results for the 3-component system when $\beta \neq 1$.

The two-species model (1.2) inherits spike solutions from (1.4), but has a much richer structure. Indeed, given any two non-negative integers k_1, k_2, there exist a solution with a total $N = k_1 + k_2$ spikes corresponding to k_1 spikes in u_1 and k_2 spikes in u_2. We shall refer to this as a (k_1, k_2) pattern.

At first glance, given N spikes, there is a total of 2^N possible ways to choose their type (each spike can be either u_1 or u_2 − type). One might then think that there is a total of 2^N possible patterns with different spike height and radius. However it turns out that the spike *ordering* of spots does not matter: only the total number of each type matters. As such, there are $N + 1$ patterns with distinct spike heights for fixed N. This is illustrated in Figure 1 which shows two distinct orderings for same number of parameters and number of spikes. Both orderings, however, have the same height and profile for the spikes u_1 and u_2.

In Figure 1, the "thirsty" patches are shown in blue and correspond to u_1 whereas the "frugal" patches are in red, corresponding to u_2. Note that the frugal plants have bigger height; this is because they absorb less water per unit growth and hence there is more water remaining for them to grow more.

As rainfall rate a is decreased, competition of water between the plants triggers the collapse of one of the spikes in the overall pattern. This process is illustrated in Figure 2, which shows that as a is decreased, the *thirsty* spikes (in blue, corresponding to u_1) die out *first,* until only "frugal" (u_2, in red) remains. Our main goal is to study stability of this N-spike equilibria. In particular, we derive the corresponding eigenvalue problem and consider both the small eigenvalues of order $O(\varepsilon^2)$ and large eigenvalues of order $O(1)$.

We now illustrate our main results. There are three thresholds that can affect the existence and stability of (k_1, k_2) spike patterns. One is the large eigenvalue threshold a_l such that the large eigenvalue becomes unstable as a decreases below a_l. The other two thresholds are small eigenvalue thresholds associated with either intraspecific

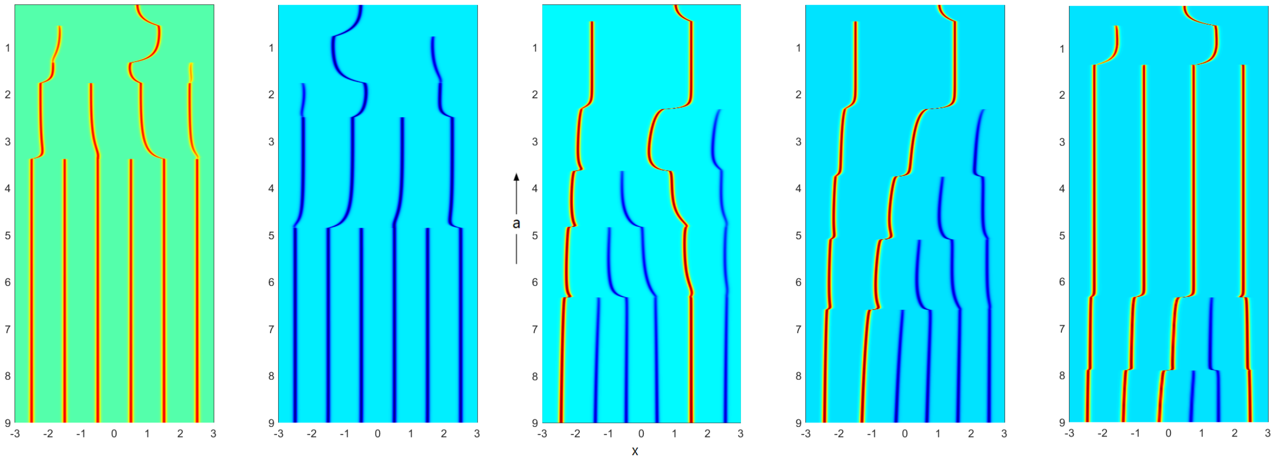

FIG. 2. Spike death as a is decreased. Here, $a = 10 - 10^{-5}t$ and other parameters are $\beta = 0.5, L = 3, D = 1, \varepsilon = 0.025$. Color plot of u_1 (“thirsty”, in blue) and u_2 (“frugal”, in red) is shown as a function of a. The subpanels only differ in initial conditions, and are arranged from most resilient pattern (on the left) to least-resilient pattern (on the right). Note that a pattern of all-frugal patches is the most resilient, followed by all-thirsty, and then mixed patterns.

competition (i.e., competition within u_1 or u_2 type) or interspecific competition (i.e., competition between u_1 and u_2 type). The intraspecific competition threshold is denoted by the fold point a_f and the interspecific competition threshold is denoted by a_s. The maximum of these three critical values gives the competition instability threshold a^*, which triggers the collapse of plant patches. By comparing a_l, a_f and a_s, we find that a_s is the dominant instability threshold for almost all (k_1, k_2) patterns except the case where only one *thirsty* spike exists (i.e., $(1, N-1)$ patterns with $\beta < 1$ and $(N-1, 1)$ patterns with $\beta > 1$) and the dominant instability threshold is a_f. This result is illustrated in Table I, where the three thresholds a_f, a_s and a_l for different (k_1, k_2) patterns are computed. The large eigenvalue threshold a_l is *dependent* of spike orderings, while the other two are not. Therefore a_f, a_s are unique for each pattern while a_l is different for different spike orderings. In Table I, we compute maximum of a_l and compare it with other thresholds in all types of 5 -spike patterns and 6-spike patterns, and it can be seen that the instability threshold a^* (maximum in each column) is given by either a_s or a_f. Note that the large eigenvalue threshold may not exist under the given parameter values such as the $(1, 4)$ pattern in Table I, which means the $(1, 4)$ pattern is always stable for the large eigenvalues.

For fixed N, we compared instability threshold a^* for different (k_1, k_2) spike patterns, and found that the plant with smaller water intake rate is more competitive. If $\beta < 1$ (i.e. $c_2 < c_1$), then u_2 is more competitive and one u_1-type spike will get killed when bifurcation happens unless the pattern only contains u_2-type spike initially. Otherwise u_1 is more competitive and one u_2-type spike will get killed when bifurcation occurs. Moreover, among the $N + 1$ combinations of spike patterns, homogeneous spike patterns (i.e.,$(0, N)$ pattern or $(N, 0)$ pattern) are always more stable than mixed-spike patterns. These results are shown in Table II, where the instability thresholds in terms of a are given for each (k_1, k_2) pattern. Smaller threshold a^* suggests that the corresponding pattern is more stable. As we see in Table II, the first number in each column is the minimum, which indicates that for fixed N, $(0, N)$ is the most stable pattern given that $\beta < 1$. Moreover, for mixed N-spike patterns, the more ”frugal” spikes are contained, the more unstable the pattern is.

The summary of the paper is as follows. We construct N spike equilibrium of system (1.2) in Section 2. In Section 3 we analyze the stability of N-spike equilibrium with respect to the large eigenvalues by deriving the corresponding nonlocal eigenvalue problem (NLEP), as well as the small eigenvalues by looking at asymmetric branches. The stability analysis is very similar to [14, 15] but with some key differences. We then show that the instability due to small eigenvalues is the dominant instability. In Section 4 we use numerics to explore what happens in the high-precipitaiton regime of large a, and we conclude with some open questions.

2. CONSTRUCTION OF N-SPIKE SOLUTIONS

In this section, we construct N-spike equilibria of system (1.2), which contains k_1 u_1-spikes and k_2 u_2-spikes. Since the patterns with fixed k_1, k_2 have same height and profile for u_1 and u_2, without loss of generality, we consider all u_1-type spikes located on the left side and all u_2-type spikes located on the right side. Since the same type of spikes

5-spike patterns thresholds	(4,1)	(3,2)	(2,3)	(1,4)
a_s	4.3372	4.9778	5.6471	2.3655
$\max(a_l)$	4.1362	4.7233	5.4138	DNE
a_f	2.3894	4.1053	5.3282	6.2754

6-spike patterns thresholds	(5,1)	(4,2)	(3,3)	(2,4)	(1,5)
a_s	5.5649	6.2585	6.9725	7.7247	3.1677
$\max(a_l)$	5.3832	6.0649	6.7470	7.4579	DNE
a_f	2.6816	4.7327	6.2608	7.4492	8.4342

TABLE I. Instability thresholds a_f, a_s and $\max(a_l)$ in N-spike patterns with $N = 5, 6$. The critical values in red are maximum in each column, which are the competition instability threshold a^* that triggers the collapse of one spike in the overall pattern. The parameters are $L = 3, \beta = 0.5, D = 1$.

$a^*_{(k_1,k_2)}$ N k_1	2	3	4	5	6
0	0.67	1.22	1.89	2.64	3.46
1	1.20	2.63	4.33	6.28	8.43
2	0.94	2.21	3.80	5.65	7.72
3		1.73	3.22	4.98	6.98
4			2.67	4.34	6.26
5				3.73	5.56
6					4.90

TABLE II. Theoretical predictions for competition instability thresholds a^* with parameters $L = 3, \beta = 0.5, D = 1$. The critical values in blue indicates the most stable patterns in each column, while the critical values in red correspond to most unstable patterns. See also Figure 2 for comparison with numerics.

has a common height and equal spacing, we define the radius of u_1-type spike as l_1 and the radius of u_2-type spike as l_2. So that l_1, l_2 satisfies

$$k_1 l_1 + k_2 l_2 = L. \tag{2.6}$$

To construct N-spike solution, we first look at inner region, where we introduce inner variable

$$y = \frac{x - x_j}{\varepsilon},$$

in which x_j is the location of j-th spike. After collecting leading order terms we have

$$\begin{aligned} u_{1yy} - u_1 + u_1^2 v &= 0, \\ u_{2yy} - u_2 + u_2^2 v &= 0, \\ v_{yy} &= 0. \end{aligned} \tag{2.7}$$

Solving system (2.7) yields

$$u_1 = \frac{1}{v_1} \sum_{j=1}^{k_1} w\left(\frac{x - x_j}{\varepsilon}\right), u_2 = \frac{1}{v_2} \sum_{j=k_1+1}^{N} w\left(\frac{x - x_j}{\varepsilon}\right), \tag{2.8}$$

in which $v_1 = v(x_j)$ with $j = 1...k_1$ and $v_2 = v(x_j)$ with $j = k_1 + 1...N$, and $w(y)$ is the "ground state" profile satisfying

$$w'' - w + w^2 = 0, \quad w'(0) = 0, \quad w(y) > 0, \quad w\,(y) \to 0 \text{ as } y \to \infty; \tag{2.9}$$

it has a well-known explicit solution

$$w(y) = \frac{3}{2}\text{sech}^2\left(\frac{y}{2}\right). \tag{2.10}$$

In the outer region, the terms that involve u_1, u_2 can be estimated as delta functions. Therefore, v satisfies

$$Dv_{xx} + a = \frac{6}{v_1}\sum_{j=1}^{k_1}\delta(x-x_j) + \frac{6\beta}{v_2}\sum_{j=k_1+1}^{N}\delta(x-x_j)\,, v_x(\pm L) = 0. \tag{2.11}$$

Here we have used the fact that $\int_{x_j^-}^{x_j^+}\frac{u_1^2 v}{\varepsilon}dx = \frac{6}{v_1}$ for $j = 1, \cdots k_1$ and $\int_{x_j^-}^{x_j^+}\frac{u_2^2 v}{\varepsilon}dx = \frac{6}{v_2}$ for $j = k_1+1, \cdots N$. Integrating equation (2.11) over $(-L, L)$ and imposing that $k_1 l_1 + k_2 l_2 = L$, we obtain

$$v_1 = \frac{3}{al_1}, v_2 = \frac{3\beta}{al_2}, \tag{2.12}$$

in which l_1, l_2 are to be determined. We then solve equation (2.11) by introducing Green's function $G(x; x_j)$ and let

$$v(x) = \bar{v} + \frac{6}{v_1}\sum_{j=1}^{k_1} G(x; x_j) + \frac{6\beta}{v_2}\sum_{j=k_1+1}^{N} G(x; x_j) \tag{2.13}$$

for some constant $\bar{v}$ to be determined. Here $G(x; x_j)$ satisfies

$$DG_{xx}(x; x_j) + \frac{1}{2L} = \delta(x - x_j), G_x(\pm L; x_j) = 0, \int_{-L}^{L} G(x; x_j) = 0, \tag{2.14}$$

which has the following solution

$$G(x; x_j) = -\frac{1}{4DL}(x^2 + x_j^2) + \frac{1}{2D}|x - x_j| - \frac{L}{6D}, j = 1, \cdots N. \tag{2.15}$$

The constant $\bar{v}$ is then determined by the matching condition $v(x_j) = v_1, j = 1, \cdots k_1$:

$$\bar{v} = v_1 - \frac{6}{v_1}\sum_{j=1}^{k_1} G(x_1; x_j) - \frac{6\beta}{v_2}\sum_{j=k_1+1}^{N} G(x_1; x_j). \tag{2.16}$$

It remains to find the radius of spikes l_1, l_2. For the patterns that only contain u_1-type or u_2-type spike (i.e., $(0, N)$ or $(N, 0)$ pattern), it is easy to see that $l_1 = l_2 = \frac{L}{N}$. For mixed-spike cases, we evaluate by matching outer solution (2.13) with inner ones $v(x_j) = v_1, j = 1, \cdots k_1$, $v(x_j) = v_2, j = k_1 + 1, \cdots N$, then we obtain

$$v_1 = \bar{v} + \frac{6}{v_1}\sum_{j=1}^{k_1} G(x_1; x_j) + \frac{6\beta}{v_2}\sum_{j=k_1+1}^{N} G(x_1; x_j), \tag{2.17}$$

$$v_2 = \bar{v} + \frac{6}{v_1}\sum_{j=1}^{k_1} G(x_N; x_j) + \frac{6\beta}{v_2}\sum_{j=k_1+1}^{N} G(x_N; x_j). \tag{2.18}$$

Note that the same type of spikes has a common height and equal spacing, so that

$$x_j = \begin{cases} -L + (2j-1)l_1, & j = 1, \cdots k_1, \\ L - (2(N-j+1)-1)l_2, & j = k_1+1, \cdots N. \end{cases} \tag{2.19}$$

Subtracting equation (2.17) from (2.18) and simplifying using equation (2.12), (2.13), and (2.15), we get

$$\frac{3\beta}{al_2} - \frac{3}{al_1} = \frac{a}{2D}(l_1^2 - l_2^2). \tag{2.20}$$

In the end, we eliminate l_1 by combining the condition $k_1 l_1 + k_2 l_2 = L$ and equation (2.20), then we obtained the following polynomial of l_2:

$$f(l_2) = el_2^4 + pl_2^3 + ql_2^2 + rl_2 + s = 0 \tag{2.21a}$$

where

$$e = (k_1^2 - k_2^2), p = 3Lk_2 - \frac{k_1^2 L}{k_2}, q = -3L^2, r = \frac{6D\beta k_1^2}{a^2} + \frac{6Dk_1^3}{a^2 k_2} + \frac{L^3}{k_2}, s = -\frac{6D\beta L k_1^2}{a^2 k_2}, \tag{2.21b}$$

and l_1 can be found through $l_1 = \frac{L - k_2 l_2}{k_1}$. We summarize our results as following:

Result 2.1 *In the limit $\varepsilon \to 0$, system (1.2) has N-spike equilibrium solution that contains k_1 u_1-spikes and k_2 u_2-spikes, in which $k_1 \geq 0$, $k_2 = N - k_1$:*

$$u_{1e}(x) = \sum_{j=1}^{k_1} \frac{w\left(\frac{x-x_j}{\varepsilon}\right)}{v_1}, \tag{2.22a}$$

$$u_{2e}(x) = \sum_{j=k_1+1}^{N} \frac{w\left(\frac{x-x_j}{\varepsilon}\right)}{v_2}, \tag{2.22b}$$

$$v_e(x) = \bar{v} + \frac{6}{v_1}\sum_{j=1}^{k_1} G(x;x_j) + \frac{6\beta}{v_2}\sum_{j=k_1+1}^{N} G(x;x_j). \tag{2.22c}$$

Here $w(y) = \frac{3}{2}\text{sech}^2\left(\frac{y}{2}\right)$, and $v_1, v_2, G(x;x_j), \bar{v}$ and x_j are given in (2.12), (2.15), (2.16), (2.19), respectively, in which l_2 can be evaluated through equation (2.21) and $l_1 = \frac{L-k_2 l_2}{k_1}$.

2.1. Fold point of N-spike equilibrium

The N-spike equilibrium has a fold point $a_f(k_1, k_2)$, corresponding to double root of the polynomial (2.21) (also referred to as the discriminant of the polynomial). It can be obtained by solving a polynomial system

$$f(l_2) = 0, f'(l_2) = 0.$$

We used Maple's grobner basis package to derive the following expression for the fold point:

$$\begin{aligned}\Delta(a) = &-256e^3s^3 + 192e^2prs^2 + 128e^2q^2s^2 - 144e^2qr^2s + 27e^2r^4 - 144ep^2qs^2 + 6ep^2r^2s + 80epq^2rs \\ &- 18epqr^3 - 16eq^4s + 4eq^3r^2 + 27p^4s^2 - 18p^3qrs + 4p^3r^3 + 4p^2q^3s - p^2q^2r^2,\end{aligned} \tag{2.23}$$

where e, p, q, r, s satisfy (2.21). Then $a_f(k_1, k_2)$ can be obtained by solving $\Delta(a_f(k_1, k_2)) = 0$ numerically.

Note that equation (2.21) is a fourth order polynomial when $k_1 \neq k_2$. When $k_1 = k_2$, it becomes a cubic polynomial and the discriminant (2.23) simplifies to

$$\Delta(a) = 27p^4s^2 - 18p^3qrs + 4p^3r^3 + 4p^2q^3s - p^2q^2r^2. \tag{2.24}$$

An example of a fold point with $k_1 = k_2 = 2$ is given in Figure 4. There are three solutions for $a > a_f$ and only one for $a < a_f$. By solving the full system (1.2) numerically, we observe that the second branch is stable when $a > a_f$; there are no stable solutions for $a < a_f$. As a consequence, the fold point a_f corresponds to one instability threshold of the system. Note that in the classical vegetation model where $\beta = 1$, the radius is unique, which is $l_1 = l_2 = \frac{L}{N}$. This matches our result shown in the right panel of Figure 4, where as $\beta = 1$, both the radius l_2 and l_1 equal to $\frac{L}{2} = 0.75$.

3. STABILITY ANALYSIS

In this section, we analyse the stability of N-spike patterns constructed in Section 2. Sec 2 2.1 shows that there are three or four branches (depending on whether $k_1 = k_2$ or not) corresponding to different equilibria. In this paper we only consider and compute stability thresholds of the stable branch such as the middle branch in Figure 4. We will first compute the bifurcation point where an asymmetric pattern bifurcates from the symmetric branch of u_1 or u_2-spike, this threshold characterizes the stability threshold of N spike equilibria with respect to the small eigenvalues with $\lambda \to 0$ as $\varepsilon \to 0$. We will then derive a Nonlocal Eigenvalue Problem (NLEP) which determines the stability of large eigenvalue ($O(1)$). Note that the large eigenvalue threshold can be affected by order of spikes, so in section 3 3.2 we consider spike steady state in general orderings. Numerical simulations are used to validate our stability results.

3.1. Asymmetric branches and competition instability thresholds

The primary mechanism that drives spike instability in one-dimensional RD models corresponds to a small-eigenvalue bifurcation [14, 15, 22]. Instead of computing fully the small eigenvalues, it was shown in [14, 15] that this bifurcation point (at which there is a zero small eigenvalue) is characterized precisely by an emergence of an asymmetric solution (e.g. two spikes of unequal height) off the symmetric branch (i.e. spikes of equal height). As expected, our two-component system inherits a similar structure, except that it has two such bifurcation points: one for each type of species which we denote by a_{s1}, a_{s2}. By taking the maximum of the two, we will obtain the bifurcation threshold $a_s = \max(a_{s1}, a_{s2})$ which is responsible for destabilization of the (k_1, k_2) pattern.

The key to computing a_{s1}, a_{s2} is to compute the value of v where $v' = 0$. These points occur inbetween any two consecutive spikes. From (2.11) we have

$$\begin{aligned} v(x_j + l_1) &\sim \tfrac{al_1^2}{2D} + \tfrac{3}{al_1}, \quad \text{when } x_j \text{ is the center of } u_1, \\ v(x_j + l_2) &\sim \tfrac{al_2^2}{2D} + \tfrac{3\beta}{al_2}, \quad \text{when } x_j \text{ is the center of } u_2. \end{aligned} \tag{3.25}$$

Since the steady state $v(x)$ is continuous, we have the following relation

$$\frac{al_1^2}{2D} + \frac{3}{al_1} = \frac{al_2^2}{2D} + \frac{3\beta}{al_2}. \tag{3.26}$$

The bifurcation point for the emergence for asymmetric u_1-spike or u_2-spike solution is obtained by calculating the minimum points in (3.25). This is given by setting $\frac{\partial}{\partial l_1}\left(\frac{al_1^2}{2D} + \frac{3}{al_1}\right) = 0$ or $\frac{\partial}{\partial l_2}\left(\frac{al_2^2}{2D} + \frac{3\beta}{al_2}\right) = 0$ for a_{s1} and a_{s2}, respectively. This yields

$$a_{s1} = \sqrt{\frac{3D}{l_1^3}}, \tag{3.27}$$

$$a_{s2} = \sqrt{\frac{3\beta D}{l_2^3}}. \tag{3.28}$$

Suppose that $\beta < 1$, then $l_1 < l_2$ and it follows that $a_{s1} > a_{s2}$. Thus $a_s = a_{s1}$, and the spike annihilation within u_1-type spike happens first. Similarly, we get $a_s = a_{s2}$ when $\beta > 1$. For the case $\beta = 1$, we have $l_1 = l_2 = \frac{L}{N}$ so that $a_s = a_{s1} = a_{s2} = \sqrt{\frac{3DN^3}{L^3}}$. This recovers the threshold previously obtained in [14, 15] for the classical Schnakenberg model. The above computations assume that there is at least two spikes of type u_1 (or u_2) when $\beta < 1$ (or $\beta > 1$). In summary, we obtain

$$a_s = \begin{cases} \sqrt{\frac{3D}{l_1^3}}, & \text{when } \beta < 1 \text{ with } k_1 \geq 2, \\ \sqrt{\frac{3\beta D}{l_2^3}}, & \text{when } \beta > 1 \text{ with } k_2 \geq 2. \end{cases} \tag{3.29}$$

Note that the threshold (3.29) computes the competition within the same type of spikes, and it does not cover the competition between u_1 and u_2 spikes. Therefore, this result does not work for $(1,1)$ pattern. However, as we compare a_s and a_f which is obtained in Section 2 2.1, we found that $a_f < a_s$ when $\beta \neq 1$, and $a_f = a_s = \sqrt{\frac{3DN^3}{L^3}}$ when $\beta = 1$. This is shown in Figure 3, where we compared a_f and a_s for $(2,2)$ and $(1,2)$ patterns. We conjecture that a_f is another small eigenvalue threshold that corresponds to interspecific competition between u_1 and u_2 spikes.

There exist two special cases: either $k_1 = 1$ (i.e., $(1, N-1)$ spike patterns) with $\beta < 1$, or $k_2 = 1$ (i.e., $(N-1, 1)$ spike patterns) with $\beta > 1$. For these cases, $a_s < a_f$, so the dominant instability is triggered by the fold point a_f as computed in Section 2 instead of a_s. This is illustrated in Figure 3, where in the left panel ($(2,2)$ pattern) $a_s = a_{s1} > a_f$, and the dominant threshold is a_s, while in the right panel ($(1,2)$ pattern) $a_f > a_s = a_{s2}$, so the dominant threshold is a_f. This is further illustrated in Figure 2, which shows an excellent agreement between numerics and theoretical results. For example, the last panel in Figure 2 shows that the first spike death is caused by $a_s = 7.7247$ in $(2,4)$ pattern and the second spike death is caused by $a_f = 6.2754$ in $(1,4)$ pattern. The theoretical thresholds a_s and a_f can be found in Table I.

3.2. Large eigenvalues and nonlocal eigenvalue problem

In this section we compute the large $O(1)$ eigenvalues by deriving the corresponding eigenvalue problem. We start by linearizing around the steady state given in (2.22). That is, we let $u_1 = u_{1e} + e^{\lambda t}\phi, u_2 = u_{2e} + e^{\lambda t}\psi$ and $v = v_e + e^{\lambda t}\xi$. Note that here the (k_1, k_2) spike steady states are considered in general spike orderings without

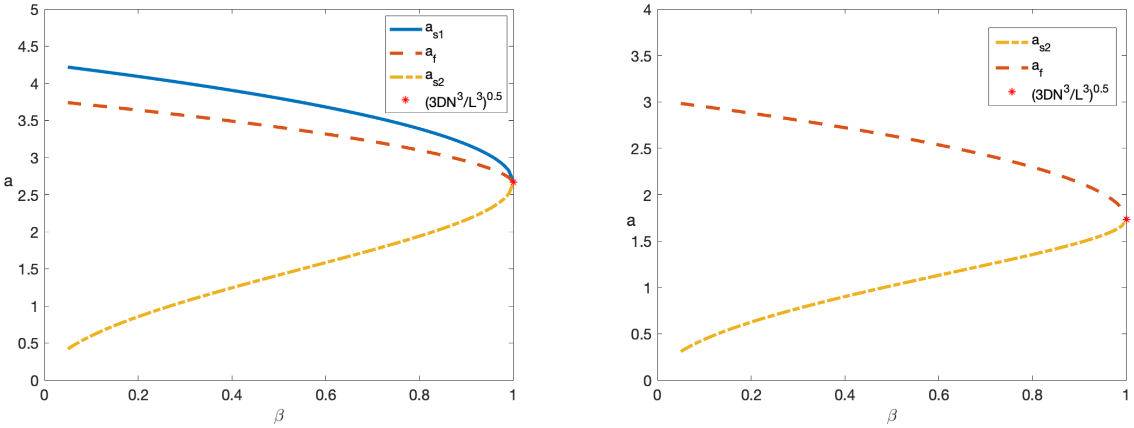

FIG. 3. Plot of three thresholds a_f (2.24), a_{s1} (3.27) and a_{s2} (3.28) vs β for $(2,2)$ spike pattern (left panel) and $(1,2)$ spike pattern (right panel). In the left figure ($(2,2)$ pattern), $a_s = a_{s1}$ is the dominant instability threshold; while on the right figure(for $(1,2)$ pattern), there is no competition within u_1 spike so only a_{s2} exist and $a_{s2} < a_f$, thus a_f is the dominant instability threshold. Here the parameters are $D = 1, L = 3$.

changing the profile of u_1 and u_2. Upon substituting into (1.2) and assuming that $|\phi| \ll 1, |\psi| \ll 1, |\xi| \ll 1$ we obtain the following eigenvalue problem

$$\lambda\phi = \varepsilon^2\phi_{xx} - \phi + 2u_{1e}v_e\phi + u_{1e}^2\xi, \quad \phi_x(\pm L) = 0, \tag{3.30a}$$

$$\lambda\psi = \varepsilon^2\psi_{xx} - \psi + 2u_{2e}v_e\phi + u_{2e}^2\xi, \quad \psi_x(\pm L) = 0, \tag{3.30b}$$

$$\tau\lambda\xi = D\xi_{xx} - \frac{1}{\varepsilon}\left[2u_{1e}v_e\phi + 2\beta u_{2e}v_e\psi + \left(u_{1e}^2 + \beta u_{2e}^2\right)\xi\right], \quad \xi_x(\pm L) = 0. \tag{3.30c}$$

Near the j-th spike, we change variables $x = x_j + \varepsilon y$. To leading order, we obtain $\xi(y) \sim \xi_j := \xi(x_j)$, and in the inner variables we have

$$\lambda\phi \sim \phi_{yy} - \phi + 2w\phi + \frac{w^2}{v_1^2}\xi_j, \tag{3.31a}$$

$$\lambda\psi \sim \psi_{yy} - \psi + 2w\psi + \frac{w^2}{v_2^2}\xi_j. \tag{3.31b}$$

Considering the different order of spikes in (k_1, k_2) pattern, we look for an eigenfunction in the form

$$\Phi \sim \sum_{j=1}^{N}\Phi_j, \xi \sim \sum_{j=1}^{N}\xi_j$$

where

$$\Phi_j = \begin{cases} \phi_j = \phi\left(\frac{x-x_j}{\varepsilon}\right), & j\text{th spike is } u_1\text{-type}, \\ \psi_j = \psi\left(\frac{x-x_j}{\varepsilon}\right), & j\text{th spike is } u_2\text{-type}. \end{cases}$$

In outer region, both ϕ and ψ are assumed to be localized functions so ξ satisfies

$$\xi_{xx} - \mu^2\xi = \sum_{j=1}^{N} c_j\delta(x - x_j), \quad \xi_x(\pm L) = 0 \tag{3.32}$$

where $\mu = \sqrt{\frac{\tau\lambda}{D}}$ and c_j is defined as

$$c_j = \begin{cases} \frac{1}{D}\left(2\int_{-\infty}^{\infty} w\phi_j dy + \frac{6}{v_1^2}\xi_j\right), & j\text{th spike is } u_1\text{-type}, \\ \frac{\beta}{D}\left(2\int_{-\infty}^{\infty} w\psi_j dy + \frac{6}{v_2^2}\xi_j\right), & j\text{th spike is } u_2\text{-type}. \end{cases} \tag{3.33}$$

We first solve (3.32) and write $\xi(x)$ as

$$\xi = \sum_{j=1}^{N} c_j G^{(\mu)}(x; x_j), \tag{3.34}$$

where $G^{(\mu)}(x; x_j)$ satisfies

$$G_{xx}^{(\mu)}(x; x_j) - \mu^2 G^{(\mu)}(x; x_j) = \delta(x - x_j), \quad G_x^{(\mu)}(\pm L; x_j) = 0. \tag{3.35}$$

Solving (3.35) yields

$$G^{(\mu)}(x; x_j) = -\frac{1}{\mu \sinh(2\mu L)} \begin{cases} \cosh\left(\mu(x+L)\right)\cosh\left(\mu(x_j - L)\right), & x < x_j \\ \cosh\left(\mu(x_j+L)\right)\cosh\left(\mu(x - L)\right), & x > x_j. \end{cases} \tag{3.36}$$

Evaluating (3.34) at $x = x_j$, we obtain that

$$\xi(x_i) = \xi_i = \sum_{j=1}^{N} c_j G_{i,j}^{(\mu)},$$

where $G_{i,j}^{(\mu)} = G^{(\mu)}(x_i; x_j)$ given in (3.36). In matrix form, it can be written as

$$\vec{\xi} = \mathcal{G}^{(\mu)} \mathcal{B} \left(\frac{2}{D} \int w \vec{\Phi} dy + \frac{6}{D} \mathcal{V} \vec{\xi} \right), \tag{3.37}$$

where

$$\vec{\xi} \equiv \begin{pmatrix} \xi_1 \\ \vdots \\ \xi_N \end{pmatrix} \quad \text{and} \quad \mathcal{G}^{(\mu)} \equiv \begin{pmatrix} G_{1,1}^{(\mu)} & G_{1,2}^{(\mu)} & \cdots & G_{1,N}^{(\mu)} \\ G_{2,1}^{(\mu)} & \ddots & \cdots & G_{2,N}^{(\mu)} \\ \vdots & \vdots & \ddots & \vdots \\ G_{N,1}^{(\mu)} & G_{N,2}^{(\mu)} & \cdots & G_{N,N}^{(\mu)} \end{pmatrix}, \tag{3.38}$$

$\mathcal{B}$ and $\mathcal{V}$ are diagonal matrices with

$$\mathcal{B}_{j,j} = \begin{cases} 1, & j\text{th spike is } u_1\text{-type}, \\ \beta, & j\text{th spike is } u_2\text{-type}, \end{cases} \quad \text{and} \quad \mathcal{V}_{j,j} = \begin{cases} \frac{1}{v_1^2}, & j\text{th spike is } u_1\text{-type}, \\ \frac{1}{v_2^2}, & j\text{th spike is } u_2\text{-type}. \end{cases} \tag{3.39}$$

Solving system (3.37) we get

$$\vec{\xi} = \frac{2}{D} \left(\mathcal{I} - \frac{6}{D} \mathcal{G}^{(\mu)} \mathcal{B} \mathcal{V} \right)^{-1} \mathcal{G}^{(\mu)} \mathcal{B} \int w \vec{\Phi} dy. \tag{3.40}$$

We label $\vec{\Phi} = \vec{m}\phi_0$ and plug (3.40) into (3.31), then we have

$$\vec{m}\lambda\phi_0 = \vec{m} L_0 \phi_0 + M \vec{m} \frac{w^2 \int w\phi_0}{\int w^2}, \tag{3.41}$$

where

$$M = \frac{2\int w^2}{D} \mathcal{V} \left(\mathcal{I} - \frac{6}{D} \mathcal{G}^{(\mu)} \mathcal{B} \mathcal{V} \right)^{-1} \mathcal{G}^{(\mu)} \mathcal{B}. \tag{3.42}$$

This yields

$$\lambda\phi_0 = L_0\phi_0 + \eta w^2 \frac{\int w\phi_0}{\int w^2}, \tag{3.43}$$

where η is the eigenvalue of M given in (3.42).

Note that when $\beta = 1$, u_1, u_2 are essentially same so that $l_1 = l_2 = \frac{L}{N}$ and $v_1 = v_2 = \frac{3N}{aL}$. Then matrix M in (3.42) becomes

$$M = \frac{2\int w^2}{Dv_1^2}\left(\mathcal{I} - \frac{6}{Dv_1^2}\mathcal{G}^{(\mu)}\right)^{-1}\mathcal{G}^{(\mu)}, \tag{3.44}$$

This recovers the results of large eigenvalue in two-component schnackenburg model [15].

For our system with $\beta \neq 1$, since it's hard to compute the general results for eigenvalues of M given in (3.42), here we consider a special case where there are 1 u_1-type and 1 u_2-type spikes. In this case we have

$$\begin{aligned} M &= \frac{2\int w^2}{D}\begin{pmatrix} \frac{1}{v_1^2} & 0 \\ 0 & \frac{1}{v_2^2} \end{pmatrix}\begin{pmatrix} 1 - \frac{6}{Dv_1^2}G_{1,1}^{(\mu)} & -\frac{6\beta}{Dv_2^2}G_{1,2}^{(\mu)} \\ -\frac{6}{Dv_1^2}G_{2,1}^{(\mu)} & 1 - \frac{6\beta}{Dv_2^2}G_{2,2}^{(\mu)} \end{pmatrix}^{-1}\begin{pmatrix} G_{1,1}^{(\mu)} & \beta G_{1,2}^{(\mu)} \\ G_{2,1}^{(\mu)} & \beta G_{2,2}^{(\mu)} \end{pmatrix} \\ &= C\begin{pmatrix} Dv_2^2 G_{1,1}^{(\mu)} - 6\beta\det(\mathcal{G}) & Dv_2^2\beta G_{1,2}^{(\mu)} \\ Dv_1^2 G_{2,1}^{(\mu)} & Dv_1^2\beta G_{2,2}^{(\mu)} - 6\beta\det(\mathcal{G}) \end{pmatrix}, \end{aligned} \tag{3.45}$$

where $\mathcal{G} = \begin{pmatrix} G_{1,1}^{(\mu)} & G_{1,2}^{(\mu)} \\ G_{2,1}^{(\mu)} & G_{2,2}^{(\mu)} \end{pmatrix}$ and $C = \frac{2\int w^2}{D^2 v_1^2 v_2^2 - 6\beta D v_1^2 G_{2,2}^{(\mu)} - 6Dv_2^2 G_{1,1}^{(\mu)} + 36\beta\det(\mathcal{G})}$.

In the limit $\tau \to 0$, we have $\mu \to 0$ and after some algebra matrix M can be simplified as

$$M = \frac{-2}{\beta Dv_1^2 + Dv_2^2 + 6\beta L}\begin{pmatrix} Dv_2^2 + 6\beta L & \beta Dv_2^2 \\ Dv_1^2 & \beta Dv_1^2 + 6\beta L \end{pmatrix}. \tag{3.46}$$

Computing the eigenvalues of M, we obtain that

$$\eta_1 = -2, \eta_2 = \frac{-12\beta L}{\beta Dv_1^2 + Dv_2^2 + 6\beta L}. \tag{3.47}$$

Let's recall the following lemma from [16]:

Lemma 3.1 *Consider the nonlocal eigenvalue problem*

$$\phi'' - \phi + 2w\phi - \alpha\frac{\int w\phi}{\int w^2}w^2 = \lambda\phi. \tag{3.48}$$

1) If $\alpha > 1$, then there exists a positive eigenvalue to (3.48);

2) If $\alpha < 1$, Then either $\lambda = 0$ with the eigenfunction $\phi = c_0 w'$ for some constant c_0 or

$$Re(\lambda) < 0.$$

From Lemma 3.1, we see that the critical threshold for the stability of large eigenvalue is such that

$$-1 = \frac{-12\beta L}{\beta Dv_1^2 + Dv_2^2 + 6\beta L}. \tag{3.49}$$

Plugging $v_1 = \frac{3}{al_1}, v_2 = \frac{3\beta}{al_2}$, we get the critical threshold for the stability of large eigenvalue (denoted as a_l)

$$a_l = \sqrt{\frac{3D}{2L}\left(\frac{1}{l_1^2} + \frac{\beta}{l_2^2}\right)}. \tag{3.50}$$

For more general case $N \geq 3$, large eigenvalue threshold a_l corresponds to the value of a for which the largest eigenvalue of M equals -1. Table III shows the thresholds a_l for different order of spikes in $(3,1)$ and $(3,2)$ spike patterns. Note that for different order of spikes, a_l can be different, so in Table III we denote the ordering of u_1 and u_2 as s, l. Although there are $\binom{N}{k_2}$ different spike orderings for fixed k_1, k_2, the number of instability thresholds is less than $\binom{N}{k_2}$ since the threshold is same when ordering is just flipped (for example, see Table III the large eigenvalue threshold is same for $(s\,s\,s\,l)$ and $(l\,s\,s\,s)$).

a_l patterns (k_1, k_2)	$(s\,s\,s\,l)$	$(s\,s\,l\,s)$	$(s\,l\,s\,s)$	$(l\,s\,s\,s)$
(3,1)	2.9898	2.7709	2.7709	2.9898

a_l patterns (k_1, k_2)	$(s\,s\,s\,l\,l)$	$(s\,s\,l\,s\,l)$	$(s\,s\,l\,l\,s)$	$(s\,l\,s\,s\,l)$	$(s\,l\,s\,l\,s)$	$(l\,s\,s\,s\,l)$
(3,2)	4.7233	4.4944	4.4941	4.5941	4.1552	4.7656

TABLE III. larger eigenvalue instability thresholds a_l in different spike orderings. The parameters are $L = 3, \beta = 0.5, D = 1$. Note that in the 2nd table we only show the spike orderings that have distinct thresholds.

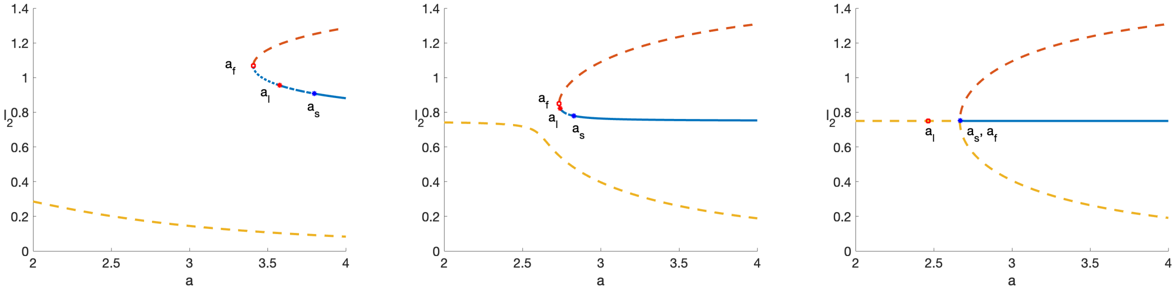

FIG. 4. Radius of u_2 spike l_2 vs a for $(2, 2)$ spike pattern. The instability thresholds on the stable branch are shown. Solid lines: linearly stable to both the small eigenvalues and the large eigenvalues; Dash-dotted lines: unstable for the small eigenvalues but stable for the large eigenvalues; Dotted line: unstable to both small eigenvalues and large eigenvalue. Here we choose $\beta = 0.5, 0.99, 0.9999$ from left to right, the other parameters are $D = 1, L = 3$.

It is well known that for two-component reaction diffusion systems the competition instability threshold in N-spike equilibria ($N \geq 2$) cross the threshold for small eigenvalues first [14, 15, 22]. And it appears to still be the case in the two-species vegetation system (1.2). We compare the instability thresholds a_l and a_s for arbitrary (k_1, k_2) patterns (except $(1, N-1)$ patterns when $\beta < 1$ and $(N-1, 1)$ patterns when $\beta > 1$) numerically; the results are shown in Figure 4, where we tried different β for $(2, 2)$ spike pattern and it is always the case $a_s > a_l$. As we increase β to 1, a_s overlaps with a_f, and a_l *does not exist* on the stable branch, which means the whole branch is stable to large eigenvalues. Similar results can be obtained for other patterns. See also Table I for more results of comparison between a_l and a_s. We then conjecture that for arbitrary (k_1, k_2) patterns it is still the case that the competition instability threshold a_s cross the threshold for small eigenvalues first.

Therefore we have $a_s > a_l$ and N-spike equilibria are stable with respect to both large and small eigenvalues when $a > a_s$; when $a_l < a < a_s$ and they are stable with respect to large eigenvalues but unstable with respect to small eigenvalues; when $a < a_l$, N-spike equilibria become unstable with respect to both large and small eigenvalues.

We now combine these results with those in Section 3 3.1. We have shown in Figure 3 that $a_s > a_f$ for $k_1 \geq 2$ ($\beta < 1$) or $k_2 \geq 2$ ($\beta > 1$) and $a_s < a_f$ for either $(1, N-1)$ spike patterns ($\beta < 1$) or $(N-1, 1)$ spike patterns ($\beta > 1$). For the former case, $a_f < a_l < a_s$, thus a_s is the dominant instability threshold; for the latter one, we found that a_l *does not exist* in the stable branch, thus $a_f > a_s$ is the dominant instability threshold.

Therefore, there are $N+1$ distinct instability thresholds denoted as a^* for each N, each corresponding to a different number of u_1 spikes (from zero to N). Moreover, we are curious about stability ordering within these patterns. We compared a^* for different $(k_1, N-k_1)$ patterns with fixed N. Table I illustrates the results for various patterns and this is further illustrated in Figure 2.

We now summarize the result as follows.

Result 3.2 *N-spike steady state to system (1.2) which contains k_1 u_1-spikes and k_2 u_2-spikes becomes unstable when a decreases to $a^* = \max(a_f, a_s)$, where a_f is the largest real root of equation (2.24) and a_s is given in equation (3.29). Moreover, using (k_1, k_2) to represent different patterns regardless of the order of different spikes, where $k_1 = 0...N, k_2 = N - k_1$, the stability of the patterns has following order (from most stable to most unstable) depending on the ratio of water intake β:*

$$\beta < 1 : (0, N) > (N, 0) > (N-1, 1) > (N-2, 2) > ... > (1, N-1),$$

$$\beta > 1 : (N, 0) > (0, N) > (1, N-1) > (2, N-2) > ... > (N-1, 1).$$

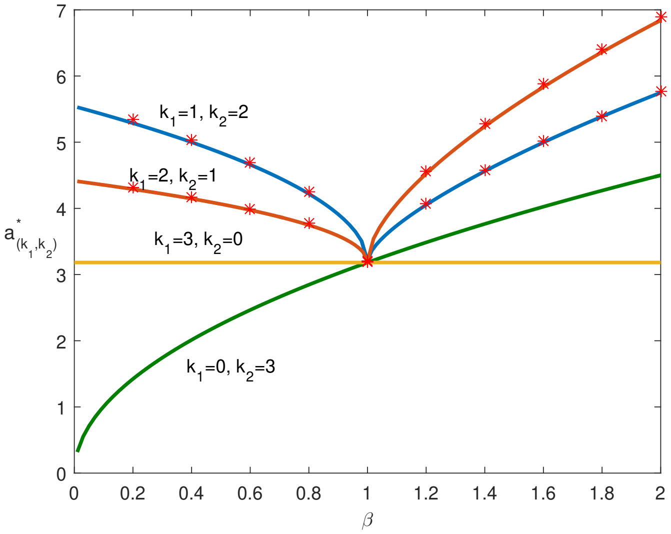

FIG. 5. Instability regions for all possible combinations of 3-spike patterns. Below each line the corresponding (k_1, k_2) pattern becomes unstable and one u_1-type spike will get killed when $k_1 \geq 1$ or one u_2-type spike get killed when $k_1 = 1$. The red dots are obtained from full simulations of system (1.2). Here the parameters are: $L = 2, D = 1, \varepsilon = 0.03$.

Figure 5 shows stability regions for all possible combinations of 3-spike patterns. As a decrease below the critical line, the corresponding pattern becomes unstable. The dots in Figure 5 are obtained by full simulations in full agreement with our analytical results.

4. DISCUSSION

We have proposed a two-species model (corresponding to two different plants), with competition for a common resource (water). This model is based on the well-known Klausmeier model of vegetation patterns. For simplicity, we concentrated on two plant species which are identical in every aspect except for the rate of water consumption: thirsty and frugal plants. We have shown that in the water-constrained regime where spike patterns exist, the two species can co-exist. However as the precipitation rate decreases, the "frugal" plant is more robust and can out-compete the more "thirsty" plant, leading to the death of thirsty plants and survival of the more frugal plant.

We found two distinct mechanisms which triggered the dominant instability, depending on the number of spikes for each type. When only one spike of the thirsty plant is present (represented in blue in Figure 2), the dominant instability corresponds to a fold point a_f as derived in Section 2 2.1, and leads to the death of the blue spike when triggered. When more than one blue spikes exists, the dominant instability corresponds to asymmetric spike bifurcation at a_s as explained in Section 3 3.1. This leads to a competition instability among the blue spikes, with one of the blue spikes getting killed. In summary, no matter which mechanism triggers spike death, the blue spikes always get killed first until only red spikes remain. In either case, when $\beta = 1$ (so that the two species are indistinguishable), the instability thresholds correspond exactly to those derived for a symmetric $N-$spike configuration for the Schnakenberg model in [14, 15]. Note that in Section 3 3.1 the conclusion that the dominant instability corresponds to asymmetric spike bifurcation at a_s rather than large eigenvalue instability threshold a_l is a conjecture. An interesting open problem is to prove it analytically.

What happens as precipitation rate is increased? For the Schnakenberg model, it is well-known that as a is increased, spot replication is observed [9, 13, 22]. A further increase of a eventually leads to a uniform-vegetation state. In the case of two species, self-replication is also observed for sufficiently large a see Figure 6 (left). However, depending on parameters, this can further lead to the more frugal plant species taking over the entire domain. This suggests that the co-existence of two plant species occurs only for precipitation parameter $a \in (a_{\text{coexistence,min}}, a_{\text{coexistence,max}})$. It is an open question to determine the upper boundary of this interval.

The behaviour of the system is very different for even larger a, as shown in Figure 7. In this case, the two plants self-organize into a propagating wave of vegetation. The red wave (corresponding to a more frugal plant) eventually

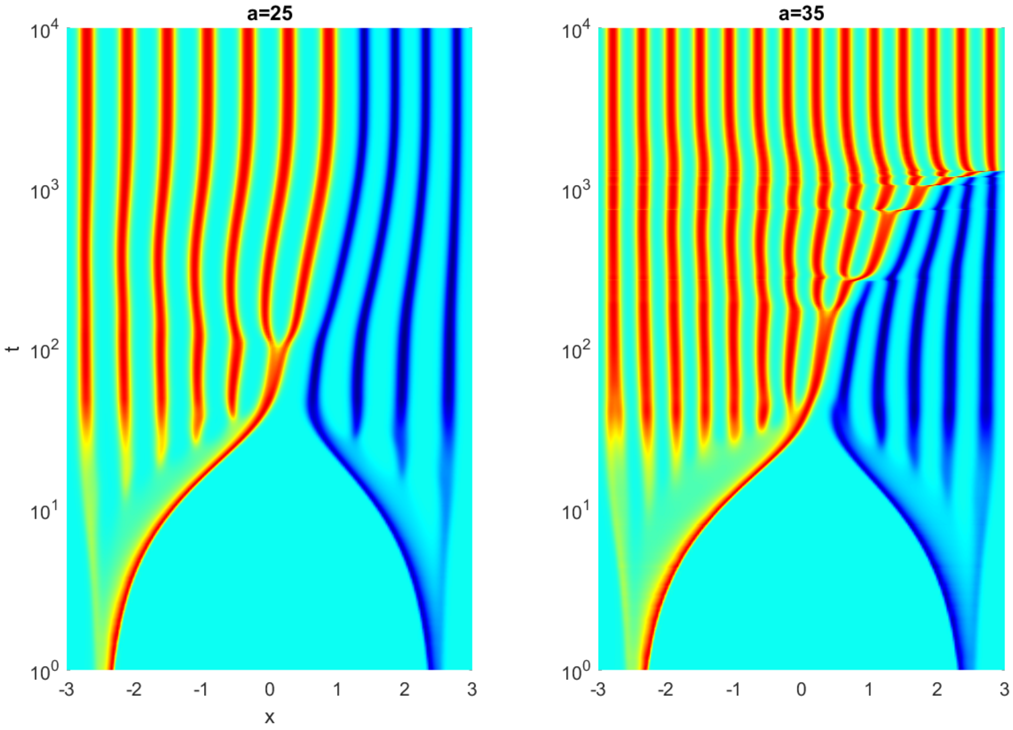

FIG. 6. Space-time plot of u_1 (blue) and u_2 (red) as a function of time with a as indicated and with $\beta = 0.6, \varepsilon = 0.03, D = 1, L = 3$. with a as indicated. Initial conditions consist of two spots on the opposite sides of the domain. Left: self-replication of both types of plants, leading to co-existence. Right: self-replication is followed by a takeover of the entire domain by the red plant. Note that time is plotted on a log scale

takes over the entire domain. An open question is compute the propagation speed as a function of system parameters.

[1] Cornelis Van Der Waal, Hans De Kroon, Willem F De Boer, Ignas MA Heitkönig, Andrew K Skidmore, Henrik J De Knegt, Frank Van Langevelde, Sipke E Van Wieren, Rina C Grant, Bruce R Page, et al. Water and nutrients alter herbaceous competitive effects on tree seedlings in a semi-arid savanna. *Journal of Ecology*, pages 430–439, 2009.

[2] DR Gordon, JM Menke, and KJ Rice. Competition for soil water between annual plants and blue oak (quercus douglasii) seedlings. *Oecologia*, 79(4):533–541, 1989.

[3] Margherita Gioria and Bruce A Osborne. Resource competition in plant invasions: emerging patterns and research needs. *Frontiers in Plant Science*, 5:501, 2014.

[4] Christopher A Klausmeier. Regular and irregular patterns in semiarid vegetation. *Science*, 284(5421):1826–1828, 1999.

[5] Olivier Lejeune, Mustapha Tlidi, and Pierre Couteron. Localized vegetation patches: a self-organized response to resource scarcity. *Physical Review E*, 66(1):010901, 2002.

[6] Ricardo Martínez-García, Justin M Calabrese, Emilio Hernández-García, and Cristóbal López. Vegetation pattern formation in semiarid systems without facilitative mechanisms. *Geophysical Research Letters*, 40(23):6143–6147, 2013.

[7] F Borgogno, P D'Odorico, F Laio, and L Ridolfi. Mathematical models of vegetation pattern formation in ecohydrology. *Reviews of Geophysics*, 47(1), 2009.

[8] K. Siteur, E. Siero, M.B. Eppinga, J.D.M. Rademacher, A. Doelman, and M. Rietkerk. Beyond Turing: The response of patterned ecosystems to environmental change. *Ecological Complexity*, 20:81–96, 2014.

[9] Yuxin Chen, Theodore Kolokolnikov, Justin Tzou, and Chunyi Gai. Patterned vegetation, tipping points, and the rate of climate change. *European Journal of Applied Mathematics*, 26(06):945–958, 2015.

[10] Jost von Hardenberg, Ehud Meron, Moshe Shachak, and Yair Zarmi. Diversity of vegetation patterns and desertification. *Physical Review Letters*, 87(19):198101, 2001.

[11] Yuval R Zelnik, Hannes Uecker, Ulrike Feudel, and Ehud Meron. Desertification by front propagation? *Journal of Theoretical Biology*, 418:27–35, 2017.

[12] Olivier Lejeune, Mustapha Tlidi, and René Lefever. Vegetation spots and stripes: dissipative structures in arid landscapes.

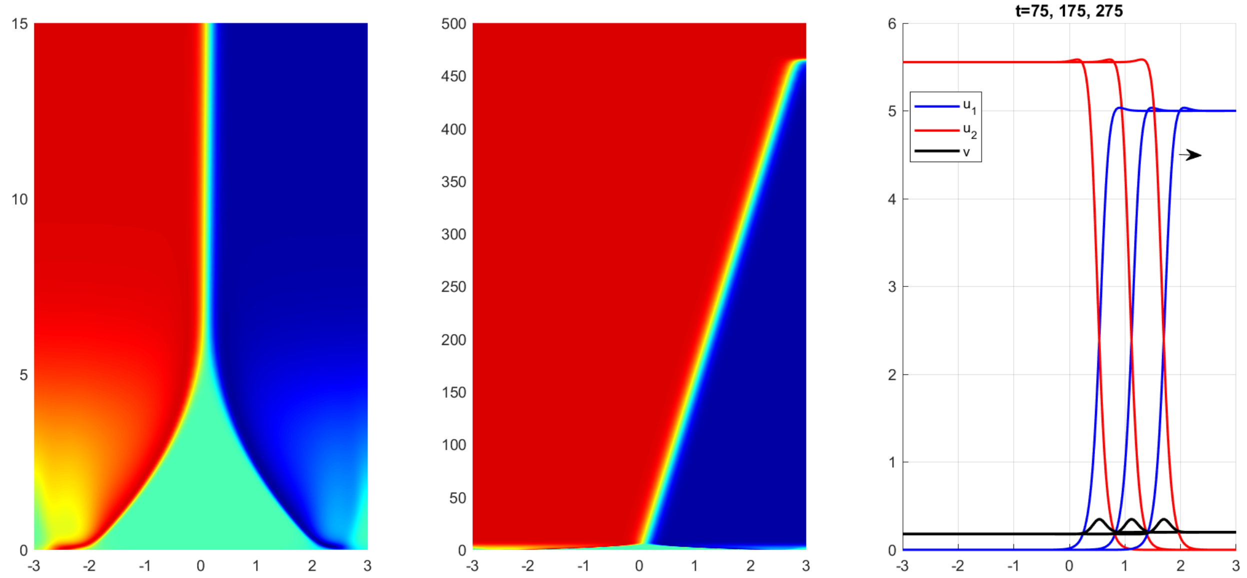

FIG. 7. Space-time plot of u_1 (blue) and u_2 (red) as a function of time with $\varepsilon = 0.1, \beta = 0.9, a = 50$. Initial conditions consist of two spots on the opposite sides of the domain. Left: intial space-filling dynamics for $t \in (0, 15)$. Middle: takeover of the domain by the red plant, $t \in (0, 500)$. Snapshot of the propagating waves at three different times as indicated. The wave propagates with a constant speed.

International Journal of Quantum Chemistry, 98(2):261–271, 2004.

[13] Karna Gowda, Yuxin Chen, Sarah Iams, and Mary Silber. Assessing the robustness of spatial pattern sequences in a dryland vegetation model. *Proceedings of the Royal Society A: Mathematical, Physical and Engineering Sciences*, 472(2187):20150893, 2016.

[14] Michael J Ward and Juncheng Wei. The existence and stability of asymmetric spike patterns for the schnakenberg model. *Studies in Applied Mathematics*, 109(3):229–264, 2002.

[15] David Iron, Juncheng Wei, and Matthias Winter. Stability analysis of turing patterns generated by the schnakenberg model. *Journal of mathematical biology*, 49(4):358–390, 2004.

[16] Juncheng Wei. On single interior spike solutions of the gierer-meinhardt system: uniqueness and spectrum estimates. *European Journal of Applied Mathematics*, 10(4):353–378, 1999.

[17] David Iron, Michael J Ward, and Juncheng Wei. The stability of spike solutions to the one-dimensional gierer–meinhardt model. *Physica D: Nonlinear Phenomena*, 150(1-2):25–62, 2001.

[18] Arjen Doelman, Tasso J Kaper, and Paul A Zegeling. Pattern formation in the one-dimensional gray-scott model. *Nonlinearity*, 10(2):523, 1997.

[19] CB Muratov and Vyacheslav V Osipov. Static spike autosolitons in the gray-scott model. *Journal of Physics A: Mathematical and General*, 33(48):8893, 2000.

[20] Cyrill B Muratov and VV Osipov. Stability of the static spike autosolitons in the gray–scott model. *SIAM Journal on Applied Mathematics*, 62(5):1463–1487, 2002.

[21] Theodore Kolokolnikov, Michael J Ward, and Juncheng Wei. The existence and stability of spike equilibria in the one-dimensional gray–scott model: The low feed-rate regime. *Studies in Applied Mathematics*, 115(1):21–71, 2005.

[22] Theodore Kolokolnikov and Juncheng Wei. Pattern formation in a reaction-diffusion system with space-dependent feed rate. *SIAM Review*, 60(3):626–645, 2018.